Astrodynamics Vol. 10, No. 1, 103–122, 2026 https://doi.org/10.1007/s42064-025-0270-8

# Dynamics modeling and optimization of an asymmetric two-stage torsion pendulum for drag-free testing in the Taiji mission

**Qifan Liu[1], Xiaokui Yue[1] (✉), Zhaohui Dang[1] (✉), Chu Zhang[2], and Yonghe Zhang[3]**

*1. School of Astronautics, Northwestern Polytechnical University, Xi'an 710072, China*
*2. Institute of Mechanics, Chinese Academy of Sciences, Beijing 710043, China*
*3. Innovation Academy for Microsatellites, Chinese Academy of Sciences, Shanghai 710699, China*

**ABSTRACT**

This paper investigates the dynamics modeling and structural optimization of an asymmetric two-stage torsion pendulum designed for drag-free testing in the Taiji mission. This torsion pendulum serves as a critical experimental apparatus for ground-based verification of drag-free control technology in space gravitational wave detection, addressing limitations in dynamic stability and parameter applicability found in traditional testbeds. Using the Lagrangian dynamics method, the equations of motion relative to inertial space are derived and simplified into a linearized dynamics model under the assumption of small-amplitude oscillations. A state-space approach is further employed to analyze the system's free oscillation behavior, with equilibrium stability rigorously assessed through eigenvalue analysis. Compared to existing approaches, the proposed model significantly enhances computational efficiency and systematically reveals the influence of key structural parameters on system stability. The study identifies critical parameter ranges essential for ensuring system stability, with optimization results demonstrating that proper design and adjustment of structural parameters can substantially improve system robustness and performance. Numerical simulations validate the accuracy of the proposed models and methods, with the optimization scheme showing clear superiority in enhancing system performance and simplifying experimental design. This work establishes a rigorous theoretical framework for ground-based verification of drag-free control technology. It not only effectively addresses bottlenecks in traditional testbed designs but also offers innovative guidance for the development of experimental systems in the Taiji mission.

**KEYWORDS**

space gravitational wave detection
two-stage torsion pendulum
drag-free
Lagrangian dynamics method

**Research Article**

Received: 16 December 2024
Accepted: 28 March 2025


## 1 Introduction

For drag-free satellites in space gravitational wave detection missions, maintaining a constant relative position and attitude between the satellite body and the freely levitating test mass (TM) inside is crucial in typical scientific mode [1, 2]. Therefore, research on the motion of the TM inside drag-free satellites is a significant aspect of dynamics study of such systems. Due to limited hardware capabilities of sensors and actuators and control methods of drag-free satellites, high-precision control of the TM can only be achieved in certain degrees of freedom (DOF) [3]. To improve control performance of the TM in drag-free satellites for space gravitational wave detection, verification experiments in a ground testing environment are necessary to reduce detection mission costs and enhance reliability of drag-free system [4]. A set of ground-based semi-physical facilities which makes motion of the TM can be measured by sensors and controlled by actuators will approximately meet drag-free condition of the TM in certain DOF, then the TM of the ground semi-physical system could exhibit dynamical similarity to that of an on-orbit drag-free satellite [5].

✉ X. Yue, xkyue@nwpu.edu.cn; Z. Dang, dangzhaohui@nwpu.edu.cn

The torsion pendulum, commonly used in experimental physics to measure minimal forces or torques, typically has a structure as shown in Fig. 1(a). The suspension fiber of torsion pendulum can effectively isolate external disturbances and reduce the impact of local gravity, because torsion torque $\boldsymbol{\Phi}$ directly reflects the effects of external torques, and suspension state provides a quasi-free fall condition. Given that a torsion pendulum can detect extremely small external torques, the effects of minimal forces and torques on the motion of experimental facilities installed on it are detectable in ground-based experimental conditions [6, 7]. Several common torsion pendulums with different structures have evolved, such as the two-point support torsion pendulum [8], the inverted torsion pendulum [9], and the double-fiber pendulum [10] shown in Figs. 1(b), 1(c), and 1(d) respectively. Except for the early applications to minimal forces and torques measurement of the Earth gravitational field [11] and gravitational constant [12], the characteristics such as torque balance and recurrent oscillation of the torsion pendulums have led to applications in measuring the inertia tensor [4, 13] and calibrating material parameters [14]. The initial applications of torsion pendulums in aerospace focused on measuring the inertia tensor [4, 10, 13] and micro-Newton thrusters [15]. Then, with the proposal of using torsion pendulums as gravitational wave detection antennas [16, 17] in recent years, the application of torsion pendulums for the ground-based experiments of space gravitational wave detection missions has gradually become a popular field [18–21]. Meanwhile, the multi-stage torsion pendulum, derived from coaxial or off-axis cascade-connection of single-stage torsion pendulums, is more sensitive in measuring of minimal forces because its DOFs of measurement and control have expanded, leading to a higher accuracy and a larger measurement range [6, 22]. As a result, this kind of multi-stage torsion pendulum has not only reduced errors in micro-newton thrusters testing [23], inertia tensor measurement [24], and material parameter calibration [25], but also enabled experiments for sensor performance testing [26] and the verification of relativistic effects [27], achieving expected results.

In space gravitational wave detection missions constructed by satellite constellations such as the Laser Interferometer Space Antenna (LISA), every drag-free satellite has two TMs inside the satellite body. A single TM can only maintain a drag-free condition in a particular sensitive DOF, while its stability in other DOFs is maintained through feedback control by external devices acting as capacitive sensors and actuators [28]. In ground-based verification experiments for space gravitational wave detection, both single-stage and multi-stage torsion pendulums have been applied to test the performance of external capacitive sensors for TMs [19], and to measure noise in torsional DOFs [29]. Ref. [30] has analyzed the impact of ground vibrations on the low-frequency motion of the torsion pendulum by comparing the results of the proposed theoretical model with the experimental measurement results. However, the research on analytical modeling and analysis for the torsion pendulum applied in ground-based drag-free verification experiments is currently insufficient. Considering the high-precision requirements of drag-free control, the current torsion pendulum dynamics models still need improvement in terms of completeness of motion and accuracy of state prediction. Moreover, due to the presence of complex disturbance signals such as ground vibrations, there is also a lack of theoretical research on the separation of the torsion pendulum motion signals and external disturbance signals in the experimental measurement results.

The Taiji Project, with its focus on drag-free control and ground semi-physical verification testing, is a space gravitational wave detection plan proposed by Chinese scientists and has been under implementation for 8 years [3]. Establishing a ground-based pure gravitational

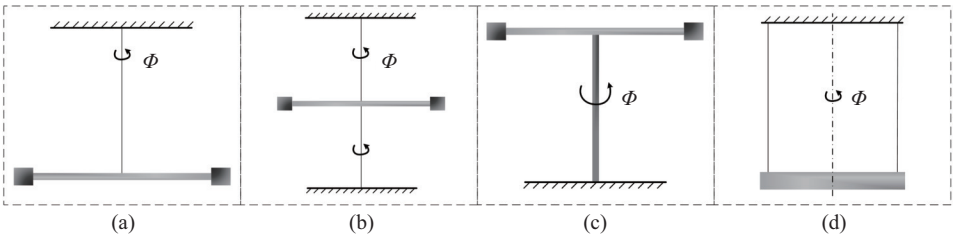


**Fig. 1** Several typical torsion pendulum structures.

environment is crucial for verifying the free-fall conditions of the Taiji drag-free system. Similar to LISA, a two-stage torsion pendulum is designed to establish this ground semi-physical verification system. However, unlike the symmetric two-stage torsion pendulum used in LISA [31], an asymmetric two-stage torsion pendulum is applied as the ground testing system for Taiji, with its structure shown in Fig. 2. By employing a non-coaxial cascading of the two-stage torsion pendulum, the entire experimental device is expected to provide the desired constrained conditions in the drag-free DOF. The study on the high precision states maintenance and transition of the TM within this two-stage torsion pendulum in drag-free DOF corresponds to the recovery of drag-free mode in the on-orbit detection system after the TM is disturbed, and the transition of drag-free states under active satellite control, respectively. The advantage of this asymmetric structure is that it simplifies the configuration of actuators and the control allocation strategy for the torsion pendulum, providing a faster control response during drag-free condition maintenance and transition. In addition, it can also reduce the coupling between different oscillation modes of torsion pendulum, especially minimizing the impact of non-torsional modes on the torsion pendulum motion [30]. Thus, the state calculation accuracy of the analytical dynamics model and error suppression in model simplification will be improved. Compared with similar ground experiments [31], this asymmetric two-stage torsion pendulum system can narrow the gap between calculation results of the analytical model and

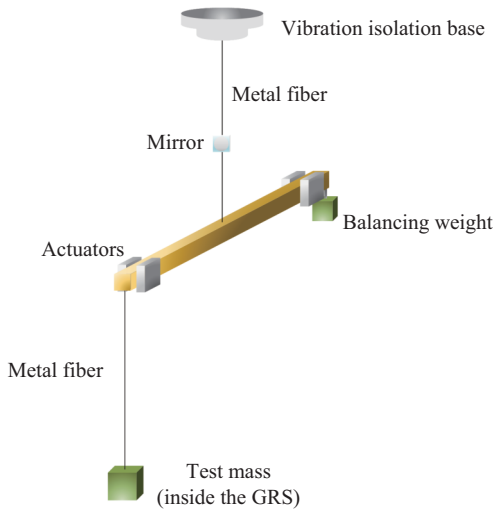


**Fig. 2** The structure of the asymmetric two-stage torsion pendulum.

the motion of the real drag-free system without drastically simplifying completeness of DOFs in dynamics analysis. It can also improve the flexibility of actuators configuration and reduce the control difficulty to achieve high-precision drag-free control.

However, this asymmetric and non-coaxial design leads to complexity of dynamic analysis at the same time, which is worthy of targeted research. During dynamics analysis, some existing two-stage torsion pendulum dynamics models are no longer suitable due to the asymmetric structure. Additionally, the frequency response characteristics and stability of this new system are also unknown. To address these problems and offer suggestions for optimizing torsion pendulum structure parameters during the design process of the ground semi-physical testing system, a dynamics model of this torsion pendulum is established to analyze its characteristics. Meanwhile, the relationships between structure parameters and dynamics model characteristics are derived by adjusting structure parameter values and analyzing the corresponding dynamics models.

The research objective of this paper is to derive the dynamics model of the asymmetric two-stage torsion pendulum for ground semi-physical verification experiments. Additionally, the study analyzes the stability of the torsion pendulum and examines the impact of its structural parameter values on system stability. The innovation of this paper lies in three key aspects:

Firstly, this study establishes a comprehensive dynamics model tailored to the asymmetric two-stage torsion pendulum, overcoming the limitations of existing models that cannot accommodate asymmetric structures. Using the Lagrangian dynamics method, a linearized representation and state-space formulation are derived, laying the foundation for analyzing dynamic behavior and optimizing system design.

Secondly, a dedicated stability analysis method is proposed for the asymmetric torsion pendulum, addressing the unique challenges posed by its structure. Through simulations and analysis of parameter variations, the study identifies critical factors affecting stability and formulates criteria for both single-parameter and multi-parameter scenarios, providing a novel approach to evaluating dynamic stability in asymmetric systems.

Thirdly, the research reveals the intrinsic relationship

between structural parameters (e.g., pendulum suspension lengths) and the system's stability. By systematically adjusting parameter values and analyzing the resulting dynamics, the study offers actionable guidance for optimizing structural parameters in semi-physical ground verification experiments, enhancing overall system performance.

Section 2 introduces the operating principle of the two-stage torsion pendulum system and examines the typical motion modes of this asymmetric structure. Section 3 derives a simplified linearized dynamics model of the two-stage torsion pendulum studied in this paper by Lagrangian dynamics and presents the system state-space model based on the linearized two-stage torsion pendulum. Section 4 introduces a stability analysis method tailored for this system and outlines the stability criteria concerning single and multiple variations in key structural parameters based on simulation experiments and analysis, which provides a deeper understanding of the system stability and a theoretical foundation for optimizing the structural parameters in the design of the two-stage torsion pendulum system. Section 5 concludes the paper by summarizing the key findings.

## 2 Preliminary analysis of the asymmetric two-stage torsion pendulum

### 2.1 Introduction to the structure and operating principles

The asymmetric two-stage torsion pendulum studied in this paper is designed for ground testing of space gravitational wave detection. It is suspended from a vibration isolation base at the top of a ground laboratory vacuum chamber, as shown in Fig. 2. Given the ultra-low-pressure environment, aerodynamic drag effects are negligible. Consequently, air resistance is excluded from dynamics modeling to simplify the analysis while maintaining fidelity to the experimental conditions. The main payload of the first-stage torsion pendulum consists of a horizontal beam that can twist around the suspended metal fiber, as well as the counterweights and the second-stage torsion pendulum, which are fixed at each end of the beam. Electrostatic actuators or micro-thrusters installed at both ends of the beam serve as driving devices to control the first-stage pendulum motion. The mirror fixed on the metal fiber, together with other optical devices in the ground laboratory, is used to accurately measure the torsion angle of the first-stage pendulum. The main payload of the second-stage torsion pendulum containing an electrode housing composed of capacitive sensing and electrostatic control devices (also known as the Gravity Reference Sensor, GRS [19]), and the freely levitating TM inside the housing.

In space gravitational wave detection missions with a multi-satellite constellation, each TM within a drag-free satellite has a single drag-free DOF, specifically oriented along the direction of the constellation network. This orientation is important for inter-satellite laser communication with another satellite's TM along the drag-free DOF. Under ideal condition, two drag-free DOFs of two TMs within a drag-free satellite form a 60° angle, as depicted in Fig. 3. Therefore, in the ground semi-physical verification system, when the horizontal beams of the two sets of two-stage torsion pendulums are placed at a 120° angle, drag-free DOF of TMs within the two sets of torsion pendulums form a 60° angle that is consistent with direction of drag-free DOFs in the on-orbit system.

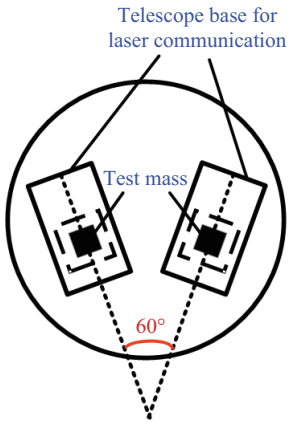


**Fig. 3** Diagram of TMs in drag-free satellite for space gravitational wave detection.

Free from perturbations and with a stationary suspension, the metal fiber of torsion pendulum exerts a tensile force that compensates the gravitational force of the TM. Thus, the drag-free DOF of TM within the two-stage torsion pendulum is perpendicular to both the horizontal beam and the suspending fiber simultaneously. The electrode housing of the pendulum is capable of monitoring all translational and rotational DOFs of the TM and controlling motion of the TM along the drag-free DOF [19] as the on-orbit detection system does. To enhance the performance of the electrode housing,

relative motion between TM and GRS can be neglected here, and the electrode housing and the freely levitating TM inside it are considered as a single entity to be the payload of the second-stage torsion pendulum. In this condition, it is possible to conduct high-fidelity semi-physical verification experiments for drag-free control while control constraints are overcome in some DOFs. Dynamics modeling and analysis of the ground-based verification facilities along the drag-free relevant DOFs provide a comprehensive understanding of the impact of the torsion pendulum structural parameters on the perturbed motion of the TM and their effect on its ability to return to a drag-free condition.

## 2.2 Structural characteristics and oscillation modes of the torsion pendulum

Based on the structure of the two-stage torsion pendulum studied, although the non-coaxial cascading gives the pendulum a distinctive asymmetric structure, certain symmetries, such as the distribution of the center of mass and the positions of actuators, are achieved under ideal stationary suspension conditions. The existence of a balancing weight block ensures that the beam of the first-stage pendulum remains horizontal and the torsion pendulum's center of mass is consistently aligned with the line that the first-stage fiber is situated along.

The main oscillation modes of a typical single-stage torsion pendulum are described across six DOFs during dynamics analysis. The motion is decomposed into 2DOFs pendulum motion modes about the upper suspension point, 2DOFs pendulum motion modes about the lower suspension point, 1DOF torsional motion mode about the suspension torsion fiber, and 1DOF elastic stretching oscillation mode along the torsion fiber. However, according to experimental measurements and theoretical analysis [32, 33], the influence of the two pendulum motion modes about the lower suspension point can be neglected in the dynamics analysis since torsional motion is the predominant mode. Besides, frictional forces at the suspension points or between fibers are explicitly omitted due to system design, which employs the rigidly fixed balancing weight and high-precision metal fibers with minimal internal damping. This simplification aligns with prior studies on torsion pendulums under vacuum conditions [6, 30], where friction can be negligible compared to torsional and gravitational effects. Thus, the motion of a single-stage torsion pendulum primarily involves four motion modes across 4DOFs.

For the two-stage torsion pendulum studied in this paper, the non-coaxial cascading structure allows actuators to be positioned at strategic points on the first-stage's beam, enabling direct control of the drag-free DOF without complex force/torque decoupling. The actuators of the first-stage pendulum typically consist of electrostatic actuating devices like parallel-plate capacitors, or reaction control system such as micro-thrusters. These actuation devices are located at opposite ends of the beam and operate simultaneously so that a control force perpendicular to the beam and passing through the suspension point of the beam can be generated to control the pendulum motion in this degree of freedom. Additionally, a force couple with its center in the suspension direction can also be generated to control the torsional motion. However, it does not enable control of the pendulum motion in another degree of freedom and the elastic oscillation motion along the torsion fiber. The electrode housing serving as the actuators of the second-stage pendulum can theoretically control the 3DOFs center of mass motion and the 3DOFs attitude motion of the TM. Nonetheless, since the electrode housing itself is suspended from the beam via the torsion fiber as the payload of the second-stage pendulum, its elastic stretching oscillation motion along the torsion fiber cannot be controlled by these actuators.

The asymmetric configuration of this two-stage torsion pendulum simplifies the actuator arrangement and control allocation strategy, enabling faster response during drag-free condition maintenance and transitions. Meanwhile, it can effectively decouple torsional motion from pendulum swing modes, reducing interference from non-drag-free DOFs and improving motion prediction accuracy. However, this asymmetric design also generates dynamics analysis complexity since the existing dynamics models for symmetric two-stage pendulums [30] are inapplicable due to asymmetric inertia and coupling terms, and deriving a tailored model is required with redefining reference coordinate systems and addressing new coupling terms.

Based on the aforementioned analysis, it is both inappropriate and complex to describe the motion of the asymmetric two-stage torsion pendulum system by the center of mass position and Euler angles when analyzing the dynamics of this system. Instead, the motion should

be described by appropriately selecting state variables related to the pendulum swing angle, torsional angle, and the extension of the metal fiber, in accordance with the typical motion modes of this asymmetric two-stage torsion pendulum system.

## 3 Dynamics modeling of the asymmetric two-stage torsion pendulum

### 3.1 Solution and linearization of dynamics model

Before modeling the dynamics of the asymmetric two-stage torsion pendulum studied in this paper, it is essential to select several appropriate reference coordinate systems based on the requirements of the dynamics analysis. As shown in Fig. 2, the first-stage pendulum comprising the beam and the balancing weight and the second-stage pendulum consisting of the TM and the electrode housing outside, together form the payload of the two-stage torsion pendulum system. To better describe and analyze the motion of the entire torsion pendulum system in inertial space, referring to LISA ground semi-physical test [18], the specific definitions of the selected reference coordinate systems are as follows.

**The inertial coordinate system $\boldsymbol{o}$**. The coordinate system origin is located at the uppermost suspension point of the torsion pendulum. The axes of this coordinate system point to the same directions as it is mentioned in Ref. [30]

**Moving coordinate system $\boldsymbol{a}$ (fixed on the first-stage torsion pendulum)**. The two-stage torsion pendulum researched in this paper has only one beam in first stage. The coordinate system origin is located at the end of the beam in the first-stage torsion pendulum, which is also the suspension point of the second-stage torsion pendulum. The $y_a$-axis is aligned along the beam, pointing towards the balancing weight, and is parallel to the $y$-axis of the inertial coordinate system $\boldsymbol{o}$ when the two-stage pendulum is in the initial equilibrium suspension state. The $z_a$-axis is always parallel to the direction of the first-stage fiber. The $x_a$-axis is perpendicular to the beam, forming a right-handed coordinate system.

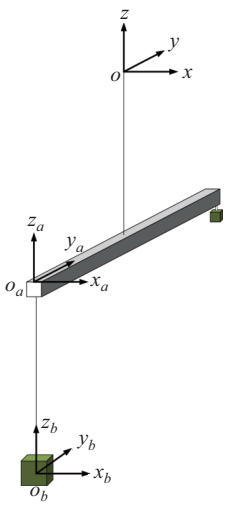


**Fig. 4** Reference coordinate systems for dynamics analysis of the asymmetric two-stage torsion pendulum.

**Moving coordinate system $\boldsymbol{b}$ (fixed on the second-stage torsion pendulum)**. The coordinate system origin coincides with the center of mass of the TM. The $x_b$-axis, $y_b$-axis, and $z_b$-axis are aligned with the three principal inertia axes of the TM, respectively. As is mentioned in Section 2, relative motion between TM and GRS is not considered. Therefore, axes directions of electrode housing are also aligned with three principal inertia axes of the TM.

In space gravitational wave detection, there is only small-amplitude motion of the TM near the drag-free state. Hence the analysis of the asymmetric two-stage torsion pendulum in a ground-based semi-physical verification system still satisfies the assumption of small-amplitude motion, namely, every DOF of the two-stage torsion pendulum exhibits only small-amplitude motion around the initial equilibrium suspension condition. Considering the DOFs involved in a single-stage torsion pendulum motion [32], some appropriate angles are chosen to describe the transformation relationship between the reference coordinate systems so that the coordinate axes are parallel to that of another frame. The inertial frame $\boldsymbol{o}$ can be transformed to the moving frame $\boldsymbol{a}$, as shown in Fig. 5, in a sequence of rotations by angles $\theta_a, \eta_a, \varphi_a$. Then the frame $\boldsymbol{a}$ is transformed in the same way to the moving frame $\boldsymbol{b}$ by angles $\theta_b, \eta_b, \varphi_b$. The coordinate transformation matrixes are denoted as $\boldsymbol{R}_{oa}$ and $\boldsymbol{R}_{ab}$, respectively.

In order to compute the system Lagrangian in Lagrange dynamics modeling, state variables that describe the current motion of the torsion pendulum will be calculated first based on unit vectors of reference frames. To concisely illustrate the physical meaning of the selected state variables, the torsion pendulum structure is

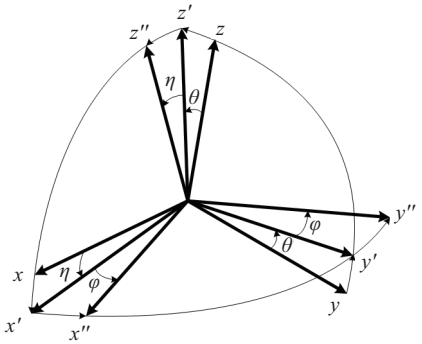


**Fig. 5** Conversion relationship of reference coordinate systems.

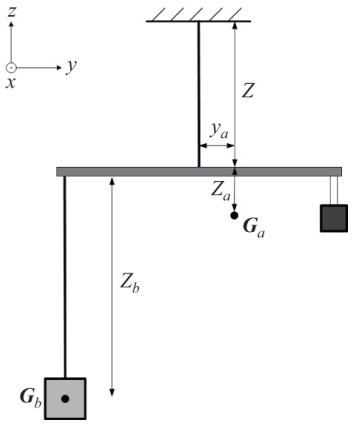


**Fig. 6** Position diagram of the center of mass of each stage torsion pendulum.

projected along the $x_a$-axis of moving frame $\boldsymbol{a}$ as shown in Fig. 6.

$G_a$ represents the position of the center of mass of the first-stage torsion pendulum which consists of the beam and balance weight. $G_b$ is the centroid position of the TM. $Z$ denotes the distance along the $z_a$-axis of moving frame $\boldsymbol{a}$ between the upper suspension point of the two-stage torsion pendulum and the beam of the first-stage pendulum, which is also the length of the first-stage suspension fiber. $Z_a$ is the distance along the $z_a$-axis of moving frame $\boldsymbol{a}$ from the center of mass $G_a$ to the beam. $Z_b$ is the distance from the center of mass $G_b$ to the upper suspension point of the second-stage torsion pendulum. $y_a$ is the lateral offset of $G_a$ to the first-stage suspension direction.

The position of $G_a$ and $G_b$ in inertial frame $\boldsymbol{o}$ are denoted as $\boldsymbol{r}_a$ and $\boldsymbol{r}_b$, respectively. $2d$ means the length of the beam. $m_a, m_b$ denote masses of the first-stage and second-stage torsion pendulum, respectively (the mass of the suspending fiber is unconsidered). The mass of the suspending fiber is neglected while the fiber still possesses elasticity and can stretch during the pendulum motion. $\delta_a, \delta_b$ represent the length changes of the suspending fibers of the first-stage and second-stage, respectively. Based on the physical meanings of these state variables of the two-stage torsion pendulum, $\boldsymbol{r}_a$ and $\boldsymbol{r}_b$ can be calculated as

$$\begin{cases} \boldsymbol{r}_a = y_a \boldsymbol{j}_a^o - (Z + Z_a + \delta_a(t))\boldsymbol{k}_a^o \\ \boldsymbol{r}_b = -(Z_b + \delta_b(t))\boldsymbol{k}_b^o - d\boldsymbol{j}_a^o - (Z + \delta_a(t))\boldsymbol{k}_a^o \end{cases} \tag{1}$$

where the subscript "$a$" and "$b$" represent unit vectors of reference frame $\boldsymbol{a}$ and $\boldsymbol{b}$, respectively. And the superscript "$o$" indicates that unit vectors are projected into the inertial frame $\boldsymbol{o}$.

Based on the Poisson formula for the time derivatives of the unit vectors of moving frames $\boldsymbol{a}$ and $\boldsymbol{b}$ [30], the angular velocities of the first-stage and second-stage pendulums with respect to the inertial frame are denoted as

$$\begin{cases} \boldsymbol{\omega}_a = \dfrac{1}{2}\left(\boldsymbol{i}_a^o \times \dfrac{\mathrm{d}\boldsymbol{i}_a^o}{\mathrm{d}t} + \boldsymbol{j}_a^o \times \dfrac{\mathrm{d}\boldsymbol{j}_a^o}{\mathrm{d}t} + \boldsymbol{k}_a^o \times \dfrac{\mathrm{d}\boldsymbol{k}_a^o}{\mathrm{d}t}\right) \\ \boldsymbol{\omega}_b = \dfrac{1}{2}\left(\boldsymbol{i}_b^o \times \dfrac{\mathrm{d}\boldsymbol{i}_b^o}{\mathrm{d}t} + \boldsymbol{j}_b^o \times \dfrac{\mathrm{d}\boldsymbol{j}_b^o}{\mathrm{d}t} + \boldsymbol{k}_b^o \times \dfrac{\mathrm{d}\boldsymbol{k}_b^o}{\mathrm{d}t}\right) \end{cases} \tag{2}$$

The Lagrangian of the studied two-stage torsion pendulum is obtained by calculating kinetic and potential energies of torsion pendulum system, which is given in Ref. [30]. However, there is some difference for torsion pendulum studied in this paper. Considering different structure of first-stage torsion pendulum, rotational inertia matrix $\boldsymbol{I}_a$ of the first-stage pendulum in the moving frame $\boldsymbol{a}$ is different numerically, but still has same form since the first-stage pendulum can be considered symmetric with respect to the plane $x_a = 0$. Then, the total kinetic energy $T$ of the system is obtained as

$$\begin{aligned} T &= K_{\mathrm{rot},a} + K_{\mathrm{rot},b} + K_{\mathrm{trans},a} + K_{\mathrm{trans},b} \\ &= \frac{1}{2}((\boldsymbol{\omega}_a^a)^{\mathrm{T}} \cdot \boldsymbol{I}_a \cdot \boldsymbol{\omega}_a^a + (\boldsymbol{\omega}_b^b)^{\mathrm{T}} \cdot \boldsymbol{I}_b \cdot \boldsymbol{\omega}_b^b \\ &\quad + m_a|\dot{\boldsymbol{r}}_a|^2 + m_b|\dot{\boldsymbol{r}}_b|^2) \end{aligned} \tag{3}$$

In accordance with the typical motion mode analysis results of the torsion pendulum system [30, 32], the calculation of the Lagrangian requires consideration of the potential energy of the two-stage torsion pendulum, which primarily consists of the gravitational potential energy of both stages, the restorative potential energy due to the torsion of the suspension fibers, and the elastic potential energy when the fibers undergo elastic extension. Consequently, the total potential energy $U$ of the two-stage torsion pendulum system is

$$U = m_a g z_{g,a} + m_b g z_{g,b} + \frac{1}{2}k_a\varphi_a^2 + \frac{1}{2}k_b\varphi_b^2 + \frac{1}{2}k_{e,a}\delta_a^2 + \frac{1}{2}k_{e,b}\delta_b^2 \tag{4}$$

where the subscripts "$a$" and "$b$" denote the respective potential energies of the first-stage and second-stage of the pendulum; $z_{g,a}, z_{g,b}$ represent the relative heights above the zero-potential-energy reference plane of the centers of mass of the first stage $G_a$ and of the TM $G_b$, respectively. When selecting the horizontal plane where the upper suspension point of the two-stage torsion pendulum is located as the zero-potential-energy reference plane, $z_{g,a}, z_{g,b}$ correspond to the $z$-axis components of $\boldsymbol{r}_a, \boldsymbol{r}_b$, respectively. $k_a, k_b$ denote the torsional spring constants of the suspension fibers for the first-stage and second-stage, respectively. $k_{e,a}, k_{e,b}$ signify the elastic coefficients for the elastic extension of the suspension fibers of the first-stage and second-stage, respectively.

Drawing from the typical motion modes considered in the dynamic analysis of a single-stage torsion pendulum [30, 32], and integrating the previously selected reference frames and coordinate transformation matrices, the Lagrangian generalized coordinate vector for the two-stage torsion pendulum system is chosen as $\boldsymbol{q} = [\theta_a, \eta_a, \varphi_a, \delta_a, \theta_b, \eta_b, \varphi_b, \delta_b]^{\mathrm{T}}$.

While solving the Lagrange equations, the process is appropriately simplified based on the assumption of small-amplitude oscillations, thereby yielding a Lagrangian dynamics model that is more concise and conducive to analyzing the pendulum motion with practical physical significance. Since all DOFs of the two-stage torsion pendulum system studied in this paper satisfy the conditions of the small-amplitude oscillation assumption, it follows that every $q_i$ is infinitesimal quantity, and its first derivative $\dot{q}_i$ and second derivative $\ddot{q}_i$ are bounded. Therefore, higher-order terms involving the product of any two or more of $q_i, \dot{q}_i, \ddot{q}_i$ can be neglected. Namely, the following assumptions hold when solving the Lagrange equations

$$\begin{cases} \sin(q_i) \approx q_i \\ \cos(q_i) \approx 1 \end{cases}, \ i = 1, 2, \cdots, 8$$

$$\begin{cases} q_i \cdot q_j \approx 0 \\ q_i \cdot \dot{q}_j \approx 0 \\ q_i \cdot \ddot{q}_j \approx 0 \end{cases}, \ i = 1, 2, \cdots, 8; \ j = 1, 2, \cdots, 8 \tag{5}$$

Substituting Eq. (5) into the Lagrange equations and solving them for each generalized coordinate, the small-amplitude oscillation assumption from Eq. (5) is applied to simplify the process, yielding the free oscillation equations of motion for the two-stage torsion pendulum system without considering control and disturbance effects as Eq. (6):

$$\frac{\mathrm{d}}{\mathrm{d}t}\left(\frac{\partial L}{\partial \dot{\boldsymbol{q}}}\right) - \frac{\partial L}{\partial \boldsymbol{q}} - \boldsymbol{Q} = 0 \tag{6}$$

where

$$\begin{cases} \boldsymbol{Q}(1) = (I_{a,1} + I_{b,1})\ddot{\theta}_a + I_{b,5}\ddot{\theta}_b + m_b d\ddot{\delta}_b + gc_1\theta_a + m_b g Z_b \theta_b \\ \boldsymbol{Q}(2) = (I_{a,2} + I_{b,2})\ddot{\eta}_a + I_{a,4}\ddot{\varphi}_a + I_{b,6}\ddot{\eta}_b + gc_1\eta_a + m_b g Z_b \eta_b \\ \boldsymbol{Q}(3) = (I_{a,3} + I_{b,3})\ddot{\varphi}_a + I_{33}^b\ddot{\varphi}_b + I_{a,4}\ddot{\eta}_a - m_b d Z_b \ddot{\eta}_b + k_a\varphi_a \\ \boldsymbol{Q}(4) = -(m_a + m_b)g + (m_a + m_b)\ddot{\delta}_a + m_b\ddot{\delta}_b + k_{e,a}\delta_a \\ \boldsymbol{Q}(5) = I_{b,5}\ddot{\theta}_a + I_{b,4}\ddot{\theta}_b + m_b g Z_b(\theta_a + \theta_b) \\ \boldsymbol{Q}(6) = I_{b,6}\ddot{\eta}_a + I_{b,7}\ddot{\eta}_b - m_b d Z_b \ddot{\varphi}_a + m_b g Z_b(\eta_a + \eta_b) \\ \boldsymbol{Q}(7) = I_{33}^b\ddot{\varphi}_a + I_{33}^b\ddot{\varphi}_b + k_b\varphi_b \\ \boldsymbol{Q}(8) = -m_b g + m_b\ddot{\delta}_a + m_b\ddot{\delta}_b + m_b d\ddot{\theta}_a + k_{e,b}\delta_b \end{cases} \tag{7}$$

From this linearized results, it is found that motion of $\delta_a$ is affected by the term $-(m_a + m_b)g$ and motion of $\delta_b$ is affected by the term $-m_b g$, which is not considered in Ref. [30]. But it makes sense since that payload weight at each stage of the torsion pendulum indeed affects system gravitational potential energy, which further affects the system Lagrangian. The detailed calculation formulas for the coefficients of certain terms in Eq. (7) can be found in Eq. (A1) in the Appendix.

Further integrating the application of the two-stage torsion pendulum in the ground-based semi-physical verification experiments for space gravitational wave detection, which is used to simulate the motion of the TM, the focus of the two-stage torsion pendulum dynamics model is on the free oscillation motion of its TM, especially the motion of the TM in the drag-free DOF. Transforming the generalized coordinates into Cartesian coordinates can more intuitively depict the motion of the TM. Similarly, based on the small-amplitude oscillation assumption, the arc length displacements due to angular changes can be approximated by translational displacements. Consequently, the position and attitude of the TM in the Cartesian inertial coordinate system can be approximated using the Lagrangian generalized coordinates as

$$x_{\mathrm{TM}} \approx -\eta_a(Z + Z_b) - \eta_b Z_b + \varphi_a d \tag{8a}$$

$$y_{\mathrm{TM}} \approx \theta_a(Z + Z_b) + \theta_b Z_b \tag{8b}$$

$$z_{\mathrm{TM}} \approx -\delta_a - \delta_b - \theta_a d \tag{8c}$$

$$\theta_{\mathrm{TM}} \approx \theta_a + \theta_b \tag{8d}$$

$$\eta_{\mathrm{TM}} \approx \eta_a + \eta_b \tag{8e}$$

$$\varphi_{\mathrm{TM}} \approx \varphi_a + \varphi_b \tag{8f}$$

where $x_{\mathrm{TM}}, y_{\mathrm{TM}}, z_{\mathrm{TM}}$ denote the position coordinates of the center of mass $G_b$ of the TM in the inertial frame $\boldsymbol{o}$. The angles $\theta_{\mathrm{TM}}, \eta_{\mathrm{TM}}, \varphi_{\mathrm{TM}}$ represent the angles between the three principal inertia axes of the TM and the $x, y, z$ axes of the inertial frame $\boldsymbol{o}$, respectively.

### 3.2 State space model of the torsion pendulum

Based on the Lagrangian dynamics model of the two-stage torsion pendulum system in Section 3.1 (Eq. (6)), it can be observed that the motion corresponding to each generalized coordinate of the two-stage torsion pendulum is influenced by one or more motion modes corresponding to other generalized coordinates, indicating that there is a coupling effect between the various channels of the two-stage torsion pendulum. To analyze the free oscillation motion resulting from the TM deviating to varying degrees from the drag-free state under the influence of different gravitational wave signals, and based on the linearized dynamics model obtained under the premise of satisfying the small-amplitude oscillation assumption, the state space model of the system is further established in the state-space to analyze its free oscillation motion characteristics.

Based on the dynamics modeling results from Eq. (6), the two-stage torsion pendulum dynamics model is a linear model with variables $\boldsymbol{q}$ and $\ddot{\boldsymbol{q}}$, and the coefficients in the equations are related solely to the structural parameters of the two-stage torsion pendulum. Therefore, the system state vector can be chosen as $\boldsymbol{x} = [\boldsymbol{q}, \dot{\boldsymbol{q}}]^{\mathrm{T}} = [\theta_a, \eta_a, \varphi_a, \delta_a, \theta_b, \eta_b, \varphi_b, \delta_b, \dot{\theta_a}, \dot{\eta_a}, \dot{\varphi_a}, \dot{\delta_a}, \dot{\theta_b}, \dot{\eta_b}, \dot{\varphi_b}, \dot{\delta_b}]^{\mathrm{T}}$, and the state equation for the two-stage torsion pendulum system, without considering control and disturbance effects, can be established as Eq. (9):

$$\dot{\boldsymbol{x}} = \begin{bmatrix} \dot{\boldsymbol{q}} \\ \ddot{\boldsymbol{q}} \end{bmatrix} = \begin{bmatrix} \boldsymbol{O}_{8\times 8} & \boldsymbol{E}_{8\times 8} \\ \boldsymbol{P}_{8\times 8} & \boldsymbol{O}_{8\times 8} \end{bmatrix} \boldsymbol{x} + \boldsymbol{b} \tag{9}$$

where $\boldsymbol{O}$ denotes the zero matrix, and $\boldsymbol{E}$ signifies the identity matrix. The matrix $\boldsymbol{P}$ and the vector $\boldsymbol{b}$ are dependent solely on the structural parameters of the two-stage torsion pendulum, the specific forms of which can be found in Eqs. (A2)–(A4) in the Appendix.

Considering the conversion between the position and attitude coordinates of the TM, as derived from Eq. (8), and the Lagrangian generalized coordinates, when the measurable position and attitude coordinates of the two-stage torsion pendulum constitute the output vector $\boldsymbol{y}$, the output equation of the two-stage torsion pendulum system can be represented as

$$\boldsymbol{y} = \begin{bmatrix} x_{\mathrm{TM}} \\ y_{\mathrm{TM}} \\ z_{\mathrm{TM}} \\ \theta_{\mathrm{TM}} \\ \eta_{\mathrm{TM}} \\ \varphi_{\mathrm{TM}} \end{bmatrix} = \begin{bmatrix} \boldsymbol{Q}_{6\times 8} & \boldsymbol{O}_{6\times 8} \end{bmatrix} \boldsymbol{x} \tag{10}$$

where $\boldsymbol{O}$ denotes the zero matrix, and the matrix $\boldsymbol{Q}$ is

$$\boldsymbol{Q} = \begin{bmatrix} 0 & -(Z+Z_b) & d & 0 & 0 & Z_b & 0 & 0 \\ Z+Z_b & 0 & 0 & 0 & Z_b & 0 & 0 & 0 \\ -d & 0 & 0 & -1 & 0 & 0 & 0 & -1 \\ 1 & 0 & 0 & 0 & 1 & 0 & 0 & 0 \\ 0 & 1 & 0 & 0 & 0 & 1 & 0 & 0 \\ 0 & 0 & 1 & 0 & 0 & 0 & 1 & 0 \end{bmatrix} \tag{11}$$

The elements of the vector $\boldsymbol{y}$ in Eq. (10) are directly measurable under idealized experimental conditions. A laser interferometry system, integrated with the mirror mounted on the asymmetric two-stage torsion pendulum (Fig. 2), enables high-precision displacement measurement. Leveraging the optical lever principle, minute displacements are amplified into resolvable angular variations, allowing precise determination of the electrode housing's position and attitude relative to the inertial frame [31]. Meanwhile, the TM's relative position and attitude within the electrode housing are monitored via capacitive sensing across multiple electrodes embedded in the housing [19]. These measurements provide real-time data on the TM's deviations from its nominal equilibrium position. Finally, utilizing the coordinate relationships defined in Section 3.1, the TM's position and attitude relative to the electrode housing are transformed into its inertial-frame coordinates $(x_{\mathrm{TM}}, y_{\mathrm{TM}}, z_{\mathrm{TM}})$ and Euler angles $(\theta_{\mathrm{TM}}, \eta_{\mathrm{TM}}, \varphi_{\mathrm{TM}})$.

Incorporating the aforementioned elements, the state space model of the two-stage torsion pendulum can be formulated as

$$\begin{cases} \dot{\boldsymbol{x}} = \boldsymbol{A}\boldsymbol{x} + \boldsymbol{b} \\ \boldsymbol{y} = \boldsymbol{C}\boldsymbol{x} \end{cases} \tag{12}$$

where

$$\boldsymbol{A}=\begin{bmatrix}\boldsymbol{O}_{8\times8} & \boldsymbol{E}_{8\times8}\\ \boldsymbol{P}_{8\times8} & \boldsymbol{O}_{8\times8}\end{bmatrix},\ \boldsymbol{C}=\begin{bmatrix}\boldsymbol{Q}_{6\times8} & \boldsymbol{O}_{6\times8}\end{bmatrix} \tag{13}$$

## 4 Stability analysis and parameters optimization

### 4.1 Stability analysis of the torsion pendulum

Stability is a prerequisite for the normal operation of a system. Therefore, when analyzing system characteristics based on the dynamics model, conducting stability analysis is an indispensable step. In this section, we will perform a stability analysis of the system based on the state space model of the two-stage torsion pendulum established in Section 3.2.

Incorporating the dynamics model of the two-stage torsion pendulum from Eq. (6) and the position and attitude calculation equations for the TM from Eq. (8), it can be deduced that when all initial values of the generalized coordinate vector $\boldsymbol{q}=[\theta_a,\eta_a,\varphi_a,\delta_a,\theta_b,\eta_b,\varphi_b,\delta_b]^{\mathrm{T}}$ are zero and control and disturbance effects are neglected, the motion state of each channel in the two-stage torsion pendulum remains unchanged. The system will always be at the equilibrium point, and the two-stage torsion pendulum will perpetually reside in its initial suspended equilibrium null position. This equilibrium state corresponds to the TM on a drag-free satellite platform in orbit being in a drag-free working condition, and in the absence of gravitational wave signals or external disturbance effects, the motion state of the TM relative to the inertial system will remain unchanged in the short term.

Based on the state space model of the two-stage torsion pendulum derived from Eq. (12), the system is a linear time-invariant continuous system under the assumption of small-amplitude oscillations and neglecting control and disturbance effects. The system matrix $\boldsymbol{A}$ and the output matrix $\boldsymbol{C}$ are uniquely determined by the structural parameters of the two-stage torsion pendulum and remain constant. Moreover, for this type of homogeneous state equation without an input vector $\boldsymbol{u}$, the solution to the state equation can describe the free motion of the system influenced solely by the initial state, which includes the free oscillation motion of the TM in the two-stage torsion pendulum system after deviating from the ideal state of undisturbed stationary suspension. Furthermore, according to the working principle of the ground-based semi-physical verification of the two-stage torsion pendulum, this zero-input response can also simulate the free oscillation motion of the TM on a drag-free satellite deviating from the drag-free state due to gravitational wave signals. However, since the right-hand side of the system state equation in Eq. (12) includes an additional constant bias vector $\boldsymbol{b}$, it is necessary to first transform the state equation of the two-stage torsion pendulum into a homogeneous equation form through an equivalent linear transformation, and then determine the stability of the two-stage torsion pendulum system based on the relationship between the eigenvalues of the system matrix and system stability.

If the system matrix $\boldsymbol{A}$ of the two-stage torsion pendulum system is non-singular, a new state vector $\boldsymbol{z}=\boldsymbol{x}+\boldsymbol{A}^{-1}\boldsymbol{b}$ is chosen in a desired form. Taking the derivative of it will obtain

$$\dot{\boldsymbol{z}}=\dot{\boldsymbol{x}}=\boldsymbol{A}\boldsymbol{x}+\boldsymbol{b}=\boldsymbol{A}(\boldsymbol{x}+\boldsymbol{A}^{-1}\boldsymbol{b})=\boldsymbol{A}\boldsymbol{z} \tag{14}$$

Thus, according to a linear transformation, a new state vector $\boldsymbol{z}$ can be selected, and the state equation describing the free motion of the two-stage torsion pendulum system can be transformed into the homogeneous equation form as shown in Eq. (14). Subsequently, the stability of the transformed system can be analyzed by solving Eq. (14) or by examining the eigenvalues of its system matrix $\boldsymbol{A}$.

However, due to the potential for the system matrix $\boldsymbol{A}$ to be singular under different parameter values of the two-stage torsion pendulum structure, the inverse of the system matrix $\boldsymbol{A}$ does not exist, making it impossible to obtain the system state equation in homogeneous form through the aforementioned linear transformation method. When the system matrix $\boldsymbol{A}$ is non-invertible, for the system state space model represented by Eq. (12), if there exists an initial value $\boldsymbol{x}_0$ of the state vector that satisfies $\boldsymbol{A}\boldsymbol{x}_0=-\boldsymbol{b}$, substituting it into the state equation yields

$$\dot{\boldsymbol{x}}_0=\boldsymbol{A}\boldsymbol{x}_0+\boldsymbol{b}=-\boldsymbol{b}+\boldsymbol{b}=\boldsymbol{0} \tag{15}$$

Therefore, in this initial state, the state of the two-stage torsion pendulum system will always remain at $\boldsymbol{x}_0$ without change, namely, $\boldsymbol{x}_0$ is an equilibrium point of the system. The prerequisite for the existence of the equilibrium point $\boldsymbol{x}_0$ under this condition is that there is an initial value of the state variable that satisfies $\boldsymbol{A}\boldsymbol{x}_0=-\boldsymbol{b}$, which means the non-homogeneous equations $\boldsymbol{A}\boldsymbol{x}=-\boldsymbol{b}$ has a solution. Thus, according to the existence and uniqueness determination conditions of the solution to

the non-homogeneous equation system, in the case of a singular system matrix $\boldsymbol{A}$, for the two-stage torsion pendulum system to have one or more equilibrium points, the system matrix $\boldsymbol{A}$ and the constant bias vector $\boldsymbol{b}$ must satisfy certain conditions.

$$\operatorname{rank}(\boldsymbol{A}) + \operatorname{rank}(\boldsymbol{b}) \geqslant n \tag{16}$$

where $n$ represents the dimension of state vector which equals to 16.

Based on the aforementioned methods for handling the system state equations under different circumstances, the procedure for the stability analysis of the two-stage torsion pendulum system is outlined in Fig. 7. The blue parts represent the important chain of case discussion, the yellow parts represent the process of the matrix equations calculation, the red parts and green parts indicate the unstable and stable cases of the system respectively.

Following the procedure outlined above, if the system matrix $\boldsymbol{A}$ is non-singular, an equivalent transformation can be performed based on the state equation from Eq. (12). By adopting a new state vector $\boldsymbol{z}$, the system state equation can be transformed into the homogeneous linear equation form, where the system matrix of the new system remains as matrix $\boldsymbol{A}$. Consequently, one should first construct the characteristic polynomial of the system matrix $\boldsymbol{A}$, solve the characteristic equation $|\lambda \boldsymbol{I} - \boldsymbol{A}|$ to obtain the eigenvalues of the system matrix, and then determine the stability of the system based on the signs of the real parts of the eigenvalues. The two-stage torsion pendulum system is considered stable if all eigenvalues have negative real parts; the system will exhibit sustained oscillatory motion if all eigenvalues have zero real parts, meaning the characteristic points are all located on the imaginary axis of the complex plane; and the system is unstable, with the free oscillation of the two-stage torsion pendulum diverging, if there is any eigenvalue with a positive real part.

## 4.2 Optimization of structural parameters on system stability

Based on the stability analysis procedure for the two-stage torsion pendulum system obtained in Section 4.1, stability analysis results can be derived for any given values of the system's structural parameters. Consequently, the method of control variables is employed to explore

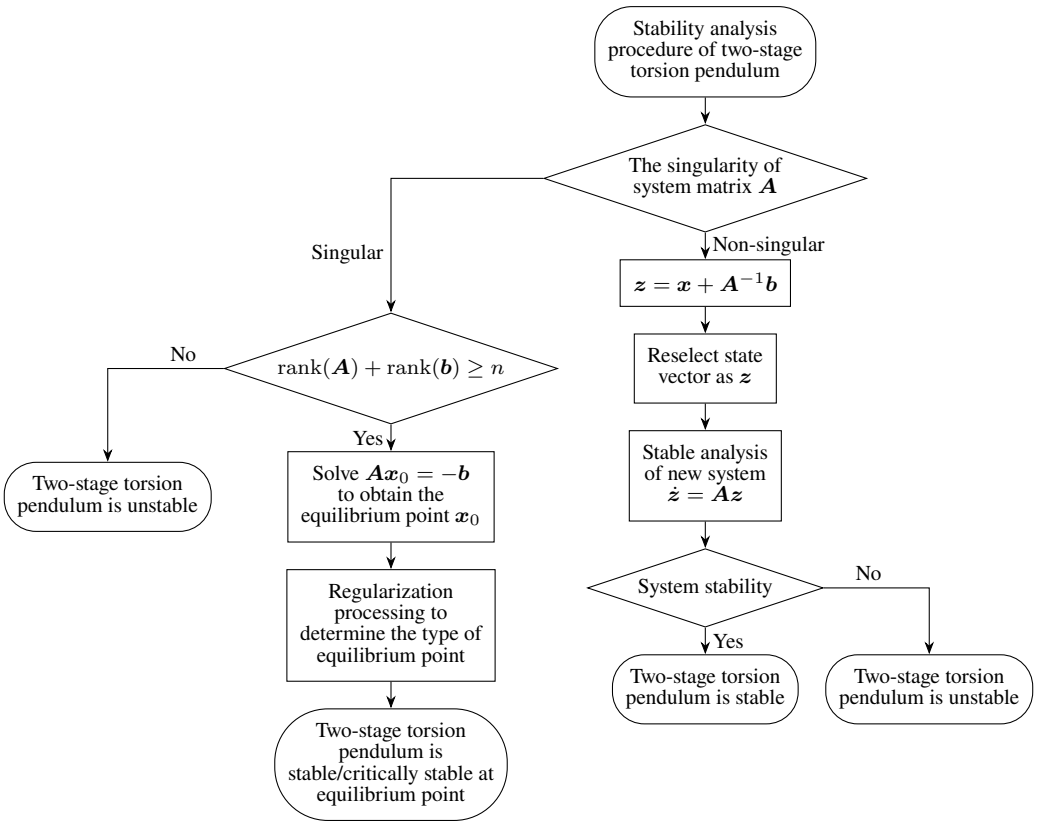


**Fig. 7** Stability analysis procedure for the asymmetric two-stage torsion pendulum system.

the patterns of stability variation under different combinations of structural parameter values, to analyze the impact of the structural parameters on the system stability. The initial values of the structural parameters for the two-stage torsion pendulum system are presented in Table 1. The nominal system structural parameter values listed in Table 1 are derived from a combination of LISA mission ground-testing systems and recalibrated values tailored to the unique asymmetric structure of the two-stage torsion pendulum for Taiji mission. Specifically, the initial parameter values are based on established configurations from LISA mission ground-based verification experiments [18, 30, 31]. These values were then adjusted to account for the asymmetric design and operational requirements of the Taiji mission.

Given the initialized structural parameters, following the stability analysis procedure for the two-stage torsion pendulum system, it is determined that the system matrix $\boldsymbol{A}$ is non-singular. Subsequently, the stability of the system can be further assessed based on the distribution pattern of the eigenvalues of the matrix $\boldsymbol{A}$. The distribution of the eigenvalues of the system matrix $\boldsymbol{A}$ under this combination of structural parameter values is illustrated in Fig. 8.

Based on the distribution of eigenvalues depicted in Fig. 8, it can be inferred that under the initialized structural parameters of the two-stage torsion pendulum, there are eigenvalues of the system matrix with non-negative real parts, indicating that the system is unstable. Consequently, when the initial state of the two-stage torsion pendulum deviates from the ideal stationary suspension state, its free oscillation motion will gradually diverge. However, due to the small real parts of the eigenvalues located in the right half of the complex plane, the rate of divergence of the system is relatively slow. When the simulation conditions are set with a non-zero value for one generalized coordinate $\varphi_{a,0} = 1^\circ$ and zero for all other generalized coordinates, the simulation results of the pendulum motion, derived from the dynamics model of the two-stage torsion pendulum system, are shown in Fig. 9.

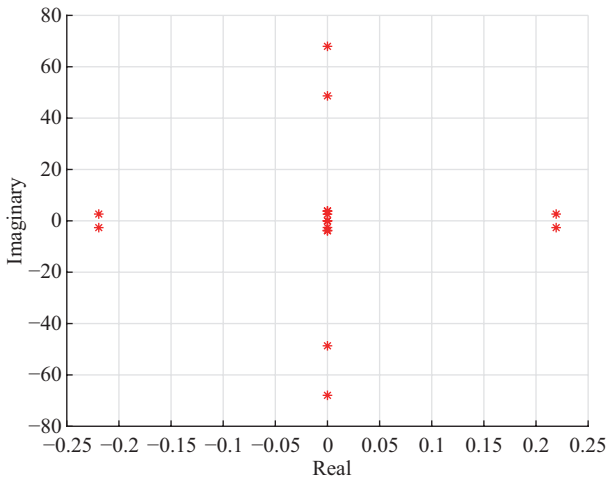


**Fig. 8** Eigenvalues distribution of system matrix $\boldsymbol{A}$ under initial structural parameter values.

To further investigate the impact of structural parameter variations on the stability of the two-stage torsion pendulum, based on the working principle of the two-stage torsion pendulum in ground verification experiments, the method of control variables is employed to study the effects of the first-stage fiber length $Z$ and the second-stage fiber length $Z_b$ on system stability, respectively.

First, the variation in the suspension length of the first-stage pendulum, that is, the change in the length of the first-stage fiber $Z$, is studied for its impact on the stability of the two-stage torsion pendulum system. Following the stability analysis procedure outlined in Section 4.1, the characteristic polynomial $|\lambda \boldsymbol{I} - \boldsymbol{A}|$ of the system matrix $\boldsymbol{A}$ is solved under the condition that the system matrix is non-singular, yielding all eigenvalues $\lambda_i$ $(i = 1, 2, \cdots, n)$ of the system matrix $\boldsymbol{A}$. The number of eigenvalues equals the dimension of the system state vector, which is $n = 16$. Subsequently, the results of the count of eigenvalues with positive real parts, negative real parts, and zero real parts as the first-stage fiber length

**Table 1** Initial structural parameter values of the torsion pendulum

$$\boldsymbol{I}_a = \begin{bmatrix} 0.165 & 0 & 0 \\ 0 & 0.106 & -5.27\times10^{-3} \\ 0 & -5.27\times10^{-3} & 2.08\times10^{-2} \end{bmatrix} \text{kg·m}^2$$

$$\boldsymbol{I}_b = \begin{bmatrix} 2.76\times10^{-6} & 0 & 0 \\ 0 & 2.77\times10^{-4} & 0 \\ 0 & 0 & 3.71\times10^{-5} \end{bmatrix} \text{kg·m}^2$$

| | |
|---|---|
| $m_a = 1.2\,\text{kg}$ | $d = 15\,\text{cm}$ |
| $m_b = 0.11\,\text{kg}$ | $k_a = 1.8\times10^{-6}\,\text{kg·m}^2/\text{s}^2$ |
| $Z = 87\,\text{cm}$ | $k_b = 7.1\times10^{-9}\,\text{kg·m}^2/\text{s}^2$ |
| $Z_a = 43\,\text{cm}$ | $k_{e,a} = 4804\,\text{kg/s}^2$ |
| $Z_b = 76\,\text{cm}$ | $k_{e,b} = 300\,\text{kg/s}^2$ |

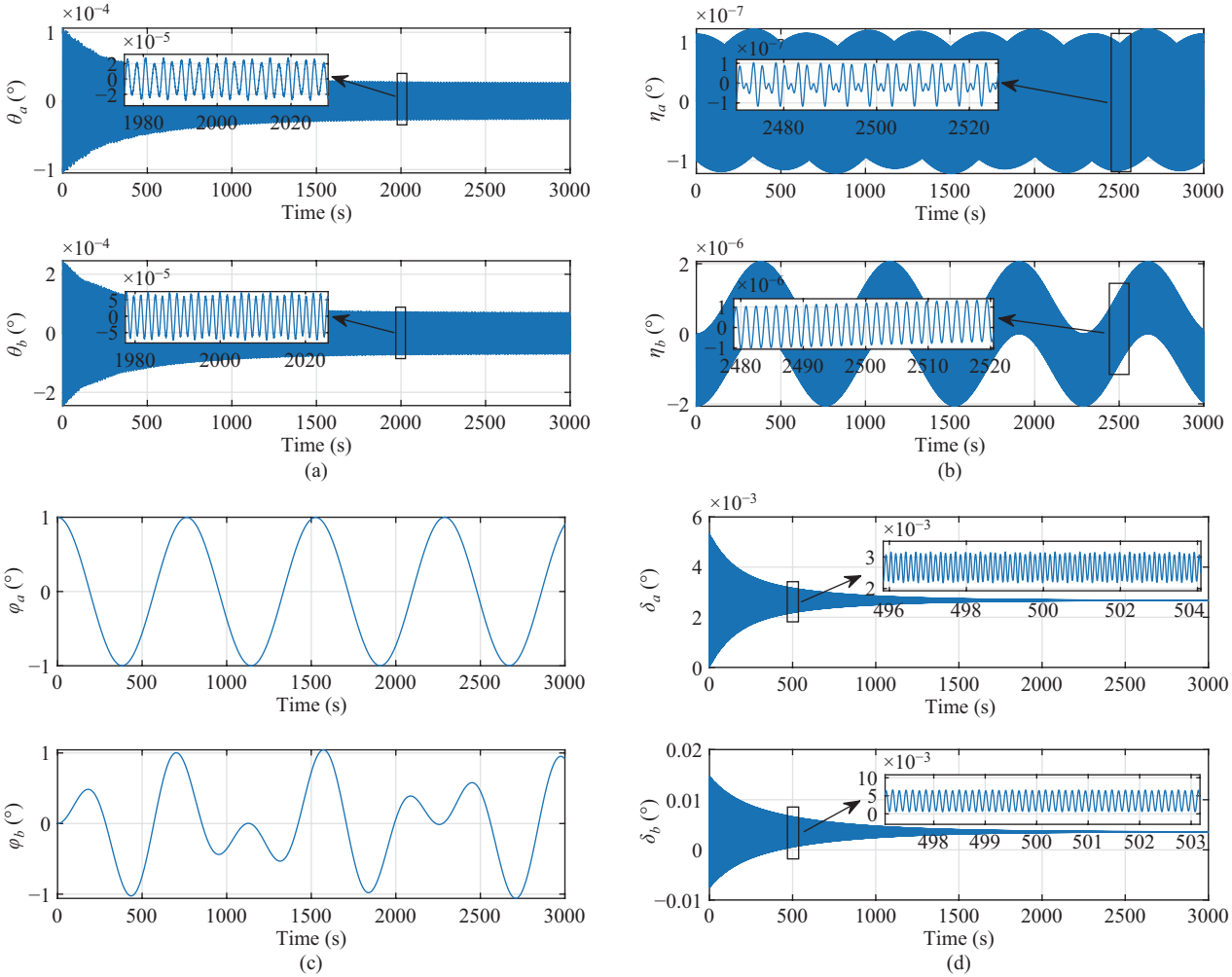


**Fig. 9** Free oscillation results of the torsion pendulum with initial structural parameters.

$Z$ varies are statistically analyzed. When the first-stage fiber length $Z$ is increased from its initial value is given in Table 1 with a step size $h = 0.0005$ m and a total of 1000 different lengths are taken, the corresponding system matrices $\boldsymbol{A}$ remain non-singular. Therefore, for each value of the fiber length $Z$, the number of eigenvalues of the matrix $\boldsymbol{A}$ with positive real parts, negative real parts, and zero real parts is obtained, as shown in Fig. 10.

During the variation process of the first-stage fiber length, changes in the structural parameter values will induce alterations in the system state space model and the system matrix $\boldsymbol{A}$ within the state space model. Upon determining that the system matrix $\boldsymbol{A}$ is non-singular, it can be observed that for any given fiber length, the number of eigenvalues with positive, negative, or zero real parts is always even. Furthermore, it is noted that the eigenvalues of the system matrix appear in conjugate pairs. Consequently, by the definition of a normal matrix, the system matrix $\boldsymbol{A}$ can be verified [34], and it is concluded that under these circumstances, the system matrix $\boldsymbol{A}$ must be a normal matrix, satisfying $\boldsymbol{A}\boldsymbol{A}^{\mathrm{H}} = \boldsymbol{A}^{\mathrm{H}}\boldsymbol{A}$, where $\boldsymbol{A}^{\mathrm{H}}$ denotes the conjugate transpose of matrix $\boldsymbol{A}$.

Furthermore, from Fig. 10, it can be observed that during the variation process of the first-stage fiber length $Z$, the distribution of 16 eigenvalues of the system, when categorized based on the sign of their real parts under the current structural parameter values, appears to be relatively random. The number of eigenvalues with a real part of zero corresponding to any given fiber length is relatively small; in most cases, fewer than four out of the 16 eigenvalues are likely to have a real part of zero. In contrast, the number of eigenvalues with positive and negative real parts is comparatively larger. Therefore, by

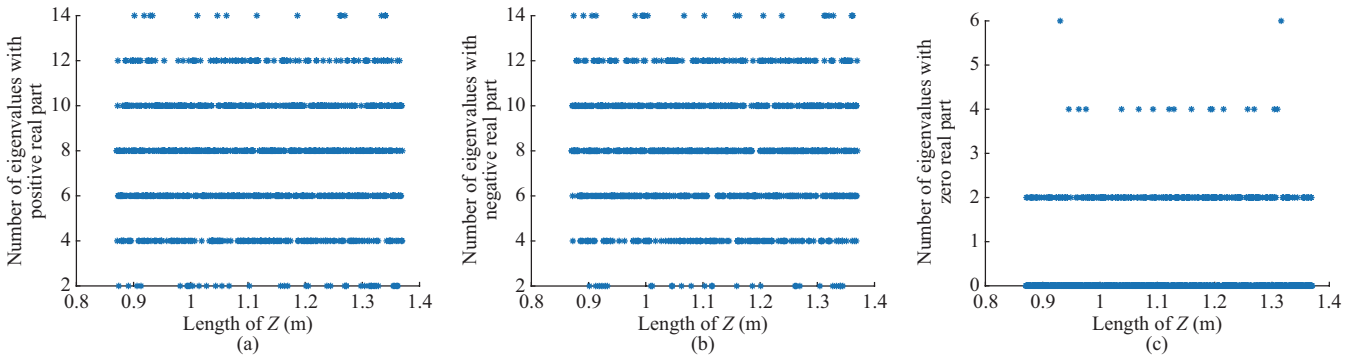


**Fig. 10** The number of eigenvalues classified by the positive and negative properties of the real part with the parameter $Z$ changing.

statistically analyzing the distribution of eigenvalues with positive and negative real parts corresponding to 1000 different values of the first-stage fiber length, a histogram of their distribution is obtained, as shown in Fig. 11.

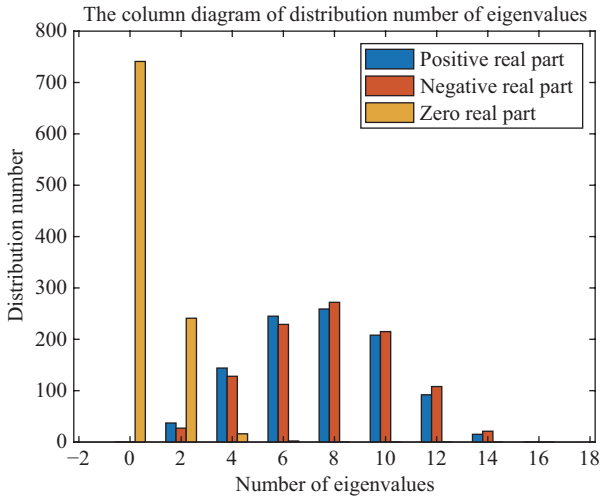


**Fig. 11** Histogram of the number distribution of eigenvalues classified by positive and negative real parts (with first stage fiber length $Z$ change).

The statistical results depicted in Fig. 11 indicate that among the 1000 possible values for the fiber length $Z$, the probability of exactly 8 out of the 16 eigenvalues of the system matrix $\boldsymbol{A}$ having a positive real part is the highest. The number of eigenvalues with a positive real part varies with different values of the first-stage fiber length $Z$, exhibiting a pattern that approximates a normal distribution. Similarly, the number of eigenvalues with a negative real part also follows a distribution pattern that changes with the fiber length $Z$.

The statistical results regarding the distribution of the number of eigenvalues were obtained under the condition that the first-stage fiber length $Z$ increases uniformly in a step $h = 0.0005$ m from an initial value $Z = 0.87$ m, with a total of 1000 different lengths being considered, thus following a uniform distribution $Z \sim U(0.87, 1.37)$. If the distribution of $Z$ is altered, the system dynamics model and the system matrix $\boldsymbol{A}$ within the state space model will undergo corresponding changes, and the distribution of the eigenvalues of the system matrix will also be affected. By adjusting the parameters of the uniform distribution that $Z$ follows, or by randomly generating values of $Z$ within a certain range of variation, one can search for cases where the number of eigenvalues with negative real parts is 16. In such cases, all eigenvalues of the system matrix $\boldsymbol{A}$ are located in the left half of the complex plane, indicating that the two-stage torsion pendulum system is stable. Therefore, this method can be used to search for parameter values within the feasible range of changes in the first-stage fiber length $Z$ that maintain system stability, thereby guiding the design of the structural parameter of the first-stage fiber length.

Following the aforementioned analytical process, the impact of variations in the second-stage fiber length $Z_b$ on the stability of the two-stage torsion pendulum system is studied, yielding similar conclusions. The length of the second-stage fiber $Z_b$ is varied starting from the initial value $Z_b = 0.76$ m that is given in Table 1, increasing uniformly in a step $h = 0.0005$ m, with a total of 1000 different lengths considered, thus following a uniform distribution $Z_b \sim U(0.76, 1.26)$. Under the condition that the system matrix $\boldsymbol{A}$ corresponding to the current value of the second-stage fiber length $Z_b$ is non-singular, it is also found that the system matrix $\boldsymbol{A}$ must be a normal matrix, with its eigenvalues appearing in conjugate pairs. Based on this, the eigenvalues of the system matrix $\boldsymbol{A}$ are

calculated and the sign of their real parts is statistically analyzed. Further statistical results indicate that among the 1000 different values of the second-stage fiber length $Z_b$, the number of eigenvalues with negative real parts among the 16 eigenvalues of the system matrix varies with different values of the second-stage fiber length $Z_b$, exhibiting a pattern that approximates a normal distribution. Therefore, by altering the distribution of the second-stage fiber length $Z_b$, one can search for parameter values within its feasible range of variation that maintain system stability, thereby optimizing the design of the structural parameter of the second-stage fiber length $Z_b$.

Based on the conclusions regarding the impact of the first-stage fiber length $Z$ and second-stage fiber length $Z_b$ on the stability of the two-stage torsion pendulum system, expanding the range of values for these two parameters and conducting a search can yield parameter values that result in all eigenvalues of the system matrix $\boldsymbol{A}$ having negative real parts. Further investigation into the simultaneous variation of these two structural parameters reveals the parameter values that maintain system stability. By searching within the range of variation for $Z \sim U(0.2, 5.2)$ and $Z_b \sim U(0.2, 10.2)$, while keeping other structural parameters at their initialized values (as shown in Table 1), the combinations of parameters that ensure system stability are obtained and illustrated in Fig. 12.

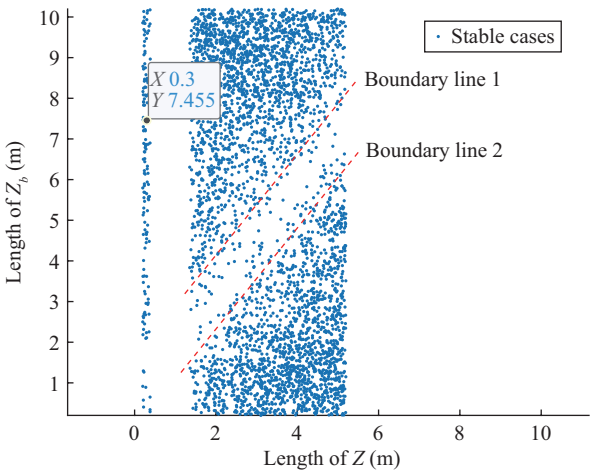


**Fig. 12** Optimal parameter values for stable two-stage torsion pendulum systems.

Based on the statistical results of the structural parameters for stable systems, it can be observed that when the parameter $Z$ takes values that are relatively small, approximately within the range of 0.2–0.3 m, the impact of the parameter $Z_b$ on system stability is comparatively weaker. Subject to the constraints of the parameter variation range set in the simulation, $Z_b$ exhibits a multitude of combinations that maintain system stability as it varies from 0.2 to 10.2 m. Furthermore, when the values of $Z$ and $Z_b$ are situated above the boundary line 1 and below the boundary line 2 in Fig. 12, and the value of $Z$ is approximately above 1.4 m, a greater number of combinations that ensure the stability of the two-stage torsion pendulum system can be obtained within the defined range. Additionally, if the search ranges for $Z$ and $Z_b$ are further expanded, the enveloped areas defined by these two sections can be broadened, implying that the range should be semi-open.

To further enhance the optimization space in the structural design of the two-stage torsion pendulum system and provide a wider range of selectable system structural parameters, considering that the distance $Z_a$ from the center of mass $G_a$ of the first-stage pendulum to the beam is determined by factors such as the mass of the beam, the mass of the counterweights, and the suspension height of the counterweights, it can offer more optimization schemes for the system structure design. Therefore, it is considered as another parameter to be optimized. By statistically analyzing the values of $Z_a$ that correspond to stable configurations of the two-stage torsion pendulum system under different value couples of $Z$ and $Z_b$, the results are illustrated in Fig. 13.

Based on the different values of the three optimization parameters when the two-stage torsion pendulum system is stable, with the value of parameter $Z_a$ determined, it is preferable to search for the values of parameter $Z$ and $Z_b$ within the envelope range defined by the corresponding red boundary line to more quickly obtain the combination of three optimized parameter values that ensure the stability of the two-stage torsion pendulum. Moreover, as the value of parameter $Z_a$ increases, the envelope range of the stable value distribution gradually shifts in the direction of decreasing parameter $Z$. Since the envelope range is a semi-open area, as the value of parameter $Z_a$ increases, it becomes easier to obtain a distribution range of stable parameter values for $Z$ and $Z_b$ that occupies a larger area in the first quadrant. Therefore, in the design of the two-stage torsion pendulum system, it can be considered to adjust factors such as the mass of the beam, the mass of the counterweights, and the suspension height of the counterweights to increase the distance $Z_a$

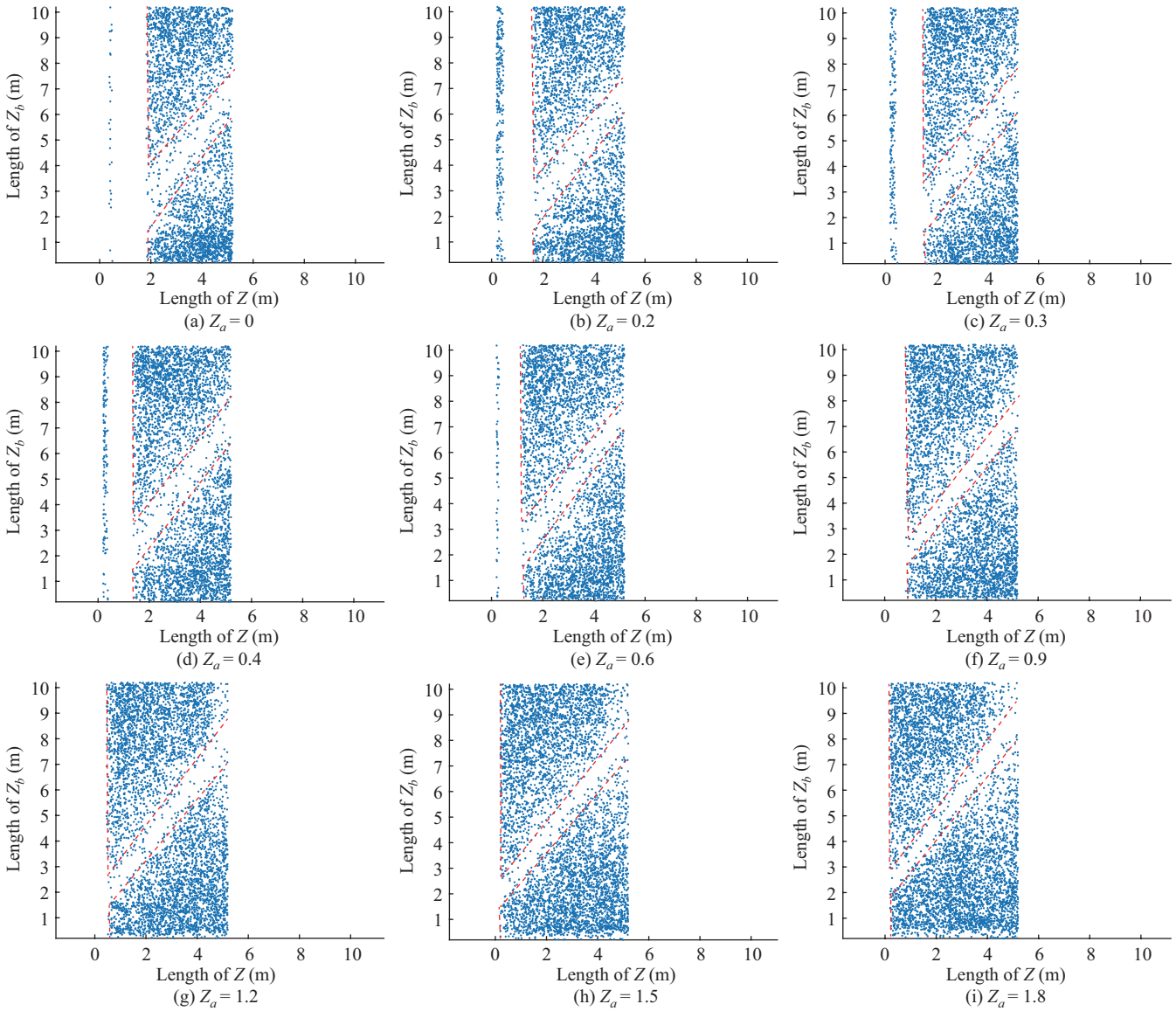


**Fig. 13** Parameters combination of stable two-stage torsion pendulum systems.

from the center of mass $G_a$ of the first-stage pendulum to the beam, thereby providing more optimization space for the values of the system structural parameters.

## 5 Conclusions

This paper focuses on an asymmetric two-stage suspended torsion pendulum designed for space-based gravitational wave detection. Under quasi-free-fall ground-based conditions, the torsion pendulum's dynamics model is established using the Lagrangian dynamics method in conjunction with its structural configuration and drag-free working conditions. Based on the reasonable assumption of small-amplitude oscillations, the model is simplified to obtain a linear model of the two-stage torsion pendulum. Subsequently, this linear model is used to describe the asymmetric system in the state space, and a stability analysis procedure for the two-stage torsion pendulum system is summarized through discussions on the different characteristics of the system's matrix. Following this analysis procedure, the system stability under the initial structural parameter values is analyzed. Then, by selecting certain structural parameters as optimization variables and examining the distribution of eigenvalues corresponding to changes in these parameters, it is observed that the distribution

of eigenvalues, categorized by the sign of their real parts, exhibits a pattern that approximates a normal distribution as the structural parameters change. Based on this, an optimization design approach is proposed to search for parameter values that ensure system stability within the feasible range of structural variables. Furthermore, multiple parameters are considered to change simultaneously to obtain combinations of parameter values that ensure system stability, and a search range for structural parameters that more readily lead to a stable system is provided, enhancing the flexibility in the design of the two-stage torsion pendulum setup. The results obtained in this paper can provide a theoretical basis for optimizing the parameter values of the drag-free satellite ground semi-physical verification system, suppressing the influence of non-primary motion modes, and thereby enhancing the dynamic similarity between the ground semi-physical verification system and the on-orbit drag-free satellite platform.

## Appendix

The calculation formulas for the coefficients of certain terms in Eq. (6) are presented as Eq. (A1):

$$\begin{cases} I_{a,1} = I_{11}^a + m_a[(Z+Z_a)^2 + y_a^2] \\ I_{a,2} = I_{22}^a + m_a(Z+Z_a)^2,\ I_{a,3} = I_{33}^a + m_a y_a^2 \\ I_{a,4} = \frac{1}{2}I_{23}^a + \frac{1}{2}I_{32}^a + m_b d(Z_a - Z_b) \\ I_{b,1} = I_{11}^b + m_b[(Z+Z_b)^2 + d^2] \\ I_{b,2} = I_{22}^b + m_b(Z+Z_b)^2,\ I_{b,3} = I_{33}^b + m_b d^2 \\ I_{b,4} = I_{11}^b + m_b Z_b^2 \\ I_{b,5} = I_{11}^b + m_b Z_b(Z+Z_b) \\ I_{b,6} = I_{22}^b + m_b Z_b(Z+Z_b),\ I_{b,7} = I_{22}^b + m_b Z_b^2 \\ c_1 = m_a(Z+Z_a) + m_b(Z+Z_b) \end{cases} \tag{A1}$$

In Eq. (9), the matrix $\boldsymbol{P}$ and the vector $\boldsymbol{b}$ are specified as Eq. (A2):

$$\boldsymbol{P} = \begin{bmatrix} \frac{k_{11}}{K_1} & 0 & 0 & \frac{k_{14}}{K_1} & \frac{k_{15}}{K_1} & 0 & 0 & \frac{k_{18}}{K_1} \\ 0 & \frac{k_{22}}{K_2} & \frac{k_{23}}{K_2} & 0 & 0 & \frac{k_{26}}{K_2} & \frac{k_{27}}{K_2} & 0 \\ 0 & \frac{k_{32}}{K_3} & \frac{k_{33}}{K_3} & 0 & 0 & \frac{k_{36}}{K_3} & \frac{k_{37}}{K_3} & 0 \\ \frac{k_{41}}{K_4} & 0 & 0 & \frac{k_{44}}{K_4} & \frac{k_{45}}{K_4} & 0 & 0 & \frac{k_{48}}{K_4} \\ \frac{k_{51}}{K_5} & 0 & 0 & \frac{k_{54}}{K_5} & \frac{k_{55}}{K_5} & 0 & 0 & \frac{k_{58}}{K_5} \\ 0 & \frac{k_{62}}{K_6} & \frac{k_{63}}{K_6} & 0 & 0 & \frac{k_{66}}{K_6} & \frac{k_{67}}{K_6} & 0 \\ 0 & \frac{k_{72}}{K_7} & \frac{k_{73}}{K_7} & 0 & 0 & \frac{k_{76}}{K_7} & \frac{k_{77}}{K_7} & 0 \\ \frac{k_{81}}{K_8} & 0 & 0 & \frac{k_{84}}{K_8} & \frac{k_{85}}{K_8} & 0 & 0 & \frac{k_{88}}{K_8} \end{bmatrix}$$

$$\boldsymbol{b} = (\overbrace{0,0,\ldots,0}^{11\text{ items}}, b_4, \overbrace{0,\ldots,0}^{4\text{ items}})^{\mathrm{T}} \tag{A2}$$

where

$$K_1 = (I_{a,1} + I_{b,1})I_{b,4}m_a - I_{b,5}^2 m_a - (m_a + m_b)I_{b,4}m_b d^2$$

$$k_{11} = I_{b,5}m_a m_b g Z_b - I_{b,4}m_a g c_1$$

$$k_{14} = -k_{e,a}I_{b,4}m_b d$$

$$k_{15} = (I_{b,5} - I_{b,4})m_a m_b g Z_b$$

$$k_{18} = (m_a + m_b)k_{e,b}I_{b,4}d$$

$$K_2 = (I_{33}^b - I_{a,3} - I_{b,3})[(I_{a,2} + I_{b,2})I_{b,7} - I_{b,6}^2] + I_{a,4}^2 I_{b,7} + 2I_{a,4}I_{b,6}m_b d Z_b + (I_{a,2} + I_{b,2})m_b^2 d^2 Z_b^2$$

$$k_{22} = (I_{a,3} + I_{b,3} - I_{33}^b)(I_{b,7}gc_1 - I_{b,6}m_b g Z_b) - (c_1 d + I_{a,4})m_b^2 g d Z_b^2$$

$$k_{23} = m_b g Z_b[(I_{a,3} + I_{b,3} - I_{33}^b)(I_{b,7} - I_{b,6}) - I_{a,4}m_b d Z_b - m_b^2 d^2 Z_b^2]$$

$$k_{26} = -k_a(I_{a,4}I_{b,7} + I_{b,6}m_b d Z_b)$$

$$k_{27} = k_b(I_{a,4}I_{b,7} + I_{b,6}m_b d Z_b)$$

$$K_3 = (I_{33}^b - I_{a,3} - I_{b,3})[(I_{a,2} + I_{b,2})I_{b,7} - I_{b,6}^2] + I_{a,4}^2 I_{b,7} + 2I_{a,4}I_{b,6}m_b d Z_b + (I_{a,2} + I_{b,2})m_b^2 d^2 Z_b^2$$

$$k_{32} = m_b g Z_b[(I_{a,2} + I_{b,2})m_b d Z_b + I_{a,4}I_{b,6}] - (I_{a,4}I_{b,7} + I_{b,6}m_b d Z_b)gc_1$$

$$k_{33} = m_b g Z_b[(I_{a,2} + I_{b,2} - I_{b,6})m_b d Z_b + (I_{b,6} - I_{b,7})I_{a,4}]$$

$$k_{36} = -k_a[I_{b,6}^2 - (I_{a,2} + I_{b,2})I_{b,7}]$$

$$k_{37} = k_b[I_{b,6}^2 - (I_{a,2} + I_{b,2})I_{b,7}]$$

$$K_4 = (I_{b,5}^2 - I_{a,1}I_{b,4} - I_{b,1}I_{b,4})m_a + (m_a + m_b)I_{b,4}m_b d^2$$

$$k_{41} = m_b g d(I_{b,4}c_1 - I_{b,5}m_b Z_b)$$

$$k_{44} = k_{e,a}(I_{a,1}I_{b,4} + I_{b,1}I_{b,4} - I_{b,4}m_b d^2 - I_{b,5}^2)$$

$$k_{45} = m_b^2 g d Z_b(I_{b,4} - I_{b,5})$$

$$k_{48} = k_{e,b}(I_{b,5}^2 - I_{b,1}I_{b,4} - I_{a,1}I_{b,4})$$

$$b_4 = (I_{b,5}^2 - I_{a,1}I_{b,4} - I_{b,1}I_{b,4})m_a g + I_{b,4}m_b g d^2(m_a + m_b)$$

$$K_5 = (I_{b,5}^2 - I_{a,1}I_{b,4} - I_{b,1}I_{b,4})m_a + (m_a + m_b)I_{b,4}m_b d^2$$

$$k_{51} = m_a g[(I_{a,1} + I_{b,1})m_b Z_b - I_{b,5}c_1] - m_b^2 g d^2 Z_b(m_a + m_b)$$

$$k_{54} = -k_{e,a}I_{b,5}m_b d$$

$$k_{55} = m_a m_b g Z_b(I_{a,1} + I_{b,1} - I_{b,5}) - m_b^2 g d^2 Z_b(m_a + m_b)$$

$$k_{58} = k_{e,b}I_{b,5}d(m_a + m_b)$$

$$K_6 = (I_{33}^b - I_{a,3} - I_{b,3})[(I_{a,2} + I_{b,2})I_{b,7} - I_{b,6}^2] + I_{a,4}^2 I_{b,7} + 2I_{a,4}I_{b,6}m_b d Z_b + (I_{a,2} + I_{b,2})m_b^2 d^2 Z_b^2$$

$$k_{62} = (I_{33}^b - I_{a,3} - I_{b,3})I_{b,6}gc_1 + [(I_{a,2} + I_{b,2})(I_{a,3} + I_{b,3} - I_{33}^b) - I_{a,4}c_1 d - I_{a,4}^2]m_b g Z_b$$

$$
\begin{aligned}
k_{63} &= k_a[I_{a,4}I_{b,6} + (I_{a,2} + I_{b,2})m_b dZ_b] \\
k_{66} &= [(I_{a,2} + I_{b,2} - I_{b,6})(I_{a,3} + I_{b,3} - I_{33}^b) \\
&\quad - I_{a,4}^2 - I_{a,4}m_b dZ_b]m_b g Z_b \\
k_{67} &= -k_b[I_{a,4}I_{b,6} + (I_{a,2} + I_{b,2})m_b dZ_b] \\
K_7 &= I_{33}^b\{[I_{b,7}(I_{a,2} + I_{b,2}) - I_{b,6}^2](I_{33}^b - I_{a,3} - I_{b,3}) \\
&\quad + I_{a,4}^2 I_{b,7} + 2I_{a,4}I_{b,6}m_b dZ_b + (I_{a,2} + I_{b,2})m_b^2 d^2 Z_b^2\} \\
k_{72} &= I_{33}^b g[I_{a,4}I_{b,7}c_1 + I_{b,6}m_b Z_b(c_1 d - I_{a,4}) \\
&\quad - m_b^2 Z_b^2 d(I_{a,2} + I_{b,2})] \\
k_{73} &= k_a I_{33}^b[I_{b,6}^2 - (I_{a,2} + I_{b,2})I_{b,7}] \\
k_{76} &= I_{33}^b m_b g Z_b[I_{a,4}(I_{b,7} - I_{b,6}) \\
&\quad + (I_{b,6} - I_{a,2} - I_{b,2})m_b dZ_b] \\
k_{77} &= k_b\{(I_{a,3} + I_{b,3})[(I_{a,2} + I_{b,2})I_{b,7} - I_{b,6}^2] \\
&\quad - 2I_{a,4}I_{b,6}m_b dZ_b - I_{a,4}^2 I_{b,7} - (I_{a,2} + I_{b,2})m_b^2 d^2 Z_b^2\} \\
K_8 &= m_b(I_{a,1}I_{b,4}m_a + I_{b,1}I_{b,4}m_a - I_{b,5}^2 m_a \\
&\quad - I_{b,4}m_a m_b d^2 - I_{b,4}m_b^2 d^2) \\
k_{81} &= m_b g d(m_a + m_b)(I_{b,4}c_1 - I_{b,5}m_b Z_b) \\
k_{84} &= k_{e,a}m_b[(I_{a,1} + I_{b,1})I_{b,4} - I_{b,5}^2] \\
k_{85} &= m_b^2 g d Z_b(m_a + m_b)(I_{b,4} - I_{b,5}) \\
k_{88} &= k_{e,b}(m_a + m_b)[I_{b,5}^2 - (I_{a,1} + I_{b,1})I_{b,4}]
\end{aligned} \tag{A3}
$$

To simplify the notation, $p_{ij}$ represents the elements of matrix $\boldsymbol{P}$, where $i, j$ $(i = 1, 2, \cdots, 8; j = 1, 2, \cdots, 8)$ denote the row and column indices of the matrix elements, respectively. Thus, the matrix $\boldsymbol{P}$ can be expressed as

$$
\boldsymbol{P} = \begin{bmatrix}
p_{11} & 0 & 0 & p_{14} & p_{15} & 0 & 0 & p_{18} \\
0 & p_{22} & p_{23} & 0 & 0 & p_{26} & p_{27} & 0 \\
0 & p_{32} & p_{33} & 0 & 0 & p_{36} & p_{37} & 0 \\
p_{41} & 0 & 0 & p_{44} & p_{45} & 0 & 0 & p_{48} \\
p_{51} & 0 & 0 & p_{54} & p_{55} & 0 & 0 & p_{58} \\
0 & p_{62} & p_{63} & 0 & 0 & p_{66} & p_{67} & 0 \\
0 & p_{72} & p_{73} & 0 & 0 & p_{76} & p_{77} & 0 \\
p_{81} & 0 & 0 & p_{84} & p_{85} & 0 & 0 & p_{88}
\end{bmatrix} \tag{A4}
$$

## Acknowledgements

This research was supported by National Key R&D Program of China: Gravitational Wave Detection Project (Grant Nos. 2021YFC22026, 2021YFC2202603, and 2021YFC2202604) and National Natural Science Foundation of China (Grant No. 12172288).

## Declaration of competing interest

The authors have no competing interests to declare that are relevant to the content of this article.

## References

[1] Jiao, B. H., Liu, Q. F., Dang, Z. H., Yue, X. K., Zhang, Y. H., Xia, Y. Q., Duan, L., Hu, Q. L., Yue, C. L., Wang, P. C., *et al.* A review on DFACS (I): System design and dynamics modeling. *Chinese Journal of Aeronautics*, **2024**, 37(5): 92–119.

[2] Yue, C. L., Jiao, B. H., Dang, Z. H., Yue, X. K., Zhang, Y. H., Xia, Y. Q., Duan, L., Hu, Q. L., Liu, Q. F., Wang, P. C., *et al.* A review on DFACS (II): Modeling and analysis of disturbances and noises. *Chinese Journal of Aeronautics*, **2024**, 37(5): 120–147.

[3] Wu, S. F., Sun, X. Y., Zhang, Q. Y., Xiang, Y. Advances in frontier research of space gravitational wave detection spacecraft platform system. *Journal of Deep Space Exploration*, **2023**, 10(3): 231–246. (in Chinese)

[4] Wang, J., Zheng, L., Zhang, X. L., Li, Z. H., Zhou, Q. C. Torsion pendulum measurement method for time varying moment of inertia. *Measurement Science and Technology*, **2023**, 34(3): 035011.

[5] Lange, B. The drag-free satellite. *AIAA Journal*, **1964**, 2(9): 1590–1606.

[6] Gillies, G. T., Ritter, R. C. Torsion balances, torsion pendulums, and related devices. *Review of Scientific Instruments*, **1993**, 64(2): 283–309.

[7] Shimoda, T., Aritomi, N., Shoda, A., Michimura, Y., Ando, M. Seismic cross-coupling noise in torsion pendulums. *Physical Review D*, **2018**, 97(10): 104003.

[8] Yang, Y. Researches on the thrust and impulse performances of micro-Newton thrusters. Ph.D. Thesis. Huazhong University of Science and Technology, **2012**. (in Chinese)

[9] Zhu, X. F., Shui, J. P. Sensitivities of two free vibration torsion pendulums. *Review of Scientific Instruments*, **1996**, 67(12): 4235–4239.

[10] Yu, Z. H. The measurement of rotational inertia for small missiles–The method of dual-line pendulum. *Aerospace Shanghai*, **1995**, 12(1): 25–30, 55. (in Chinese)

[11] Cavendish, H. Experiments to determine the density of the Earth. by henry Cavendish, esq. F. R. S. and A. S. *Philosophical Transactions of the Royal Society of London*, **1798**, 88(1798): 469–526.

[12] Liu, J. P., Wu, J. F., Li, Q., Xue, C., Mao, D. K., Yang, S. Q., Shao, C. G., Tu, L. C., Hu, Z. K., Luo, J. Progress on the precision measurement of the Newtonian gravitational constant G. *Acta Physica Sinica*, **2018**, 67(16): 160603.

[13] Zhao, Y. Research on nonlinear problems in moment of inertia measurement based on torsion pendulum. Ph.D. Thesis. Harbin Institute of Technology, **2013**. (in Chinese)

[14] Hong, X. G., Lu, K. Q. Viscosity measurement with double-wire torsion pendulum. *Review of Scientific Instruments*, **1995**, 66(8): 4318–4325.

[15] Smith, B. J., Black, J. T., Adams, C. S. Design and calibration of a torsion pendulum for micronewton-class spacecraft thrusters. *Journal of Aerospace Engineering*, **2022**, 35(3): 04022023.

[16] Douglass, D. H., Tyson, J. A. New class of gravitational wave detectors. *Nature*, **1971**, 229(5279): 34–36.

[17] Zheng, Q. Z., Cui, S. Z. Torsional pendulum—a possible antenna for detecting low frequency gravitational waves. *Acta Physica Sinica*, **1980**, 29(9): 1204.

[18] Russano, G. A torsion pendulum ground test of the LISA Pathfinder Free-fall mode. *arXiv preprint*, **2016**, arXiv:1609.00002.

[19] Bassan, M., Cavalleri, A., De Laurentis, M., De Marchi, F., De Rosa, R., Di Fiore, L., Dolesi, R., Finetti, N., Garufi, F., Grado, A., *et al.* Actuation crosstalk in free-falling systems: Torsion pendulum results for the engineering model of the LISA pathfinder gravitational reference sensor. *Astroparticle Physics*, **2018**, 97: 19–26.

[20] Apple, S., Álvarez, A. D., Kenyon, S. P., Chilton, A., Klein, D., Bickerstaff, B., Barke, S., Clark, M., Letson, B., Olatunde, T., *et al.* Design and performance characterization of a new LISA-like (Laser Interferometer Space Antenna-like) gravitational reference sensor and torsion pendulum testbed. *Review of Scientific Instruments*, **2023**, 94(5): 054502.

[21] Zhang, C., He, J. W., Chen, M. W., Duan, L., Kang, Q. Ground semi-physical simulation experiment study of one-dimensional drag-free control. *International Journal of Modern Physics A*, **2021**, 36(11–12): 2140016.

[22] De Marchi, F., Bassan, M., Pucacco, G., Marconi, L., Stanga, R., Visco, M. Analytic model for the rototranslational torsion pendulum. In: Proceedings of the 9th International LISA Symposium, **2012**, 467: 251.

[23] Cong, L. X., Wang, J. B., Long, J. F., Mu, J. C., Deng, H. Y., Qiao, C. F. Microgravity decoupling in torsion pendulum for enhanced micro-Newton thrust measurement. *Applied Sciences*, **2024**, 14(1): 91.

[24] Su, C. Q., Lu, Z. H. Improvement of experimental identification method with trifilar torsional pendulum for inertia properties of large-scale rigid-body. *Engineering Mechanics*, **2007**, 24(7): 59–65, 71. (in Chinese)

[25] Lisowski, B., Retiere, C., Moreno, J. P. G., Olejnik, P. Semiempirical identification of nonlinear dynamics of a two-degree-of-freedom real torsion pendulum with a nonuniform planar stick–slip friction and elastic barriers. *Nonlinear Dynamics*, **2020**, 100(4): 3215–3234.

[26] Ciani, G., Chilton, A., Apple, S., Olatunde, T., Aitken, M., Mueller, G., Conklin, J. W. A new torsion pendulum for gravitational reference sensor technology development. *Review of Scientific Instruments*, **2017**, 88(6): 064502.

[27] Yue, Y., Fan, S. H., Liu, L. X., Luo, J. Dynamical behaviour of a modulated torsion pendulum in test of weak equivalence principle. *Chinese Physics Letters*, **2005**, 22(8): 1837–1840.

[28] Bayle, J. B., Bonga, B., Caprini, C., Doneva, D., Muratore, M., Petiteau, A., Rossi, E., Shao, L. J. Overview and progress on the laser interferometer space antenna mission. *Nature Astronomy*, **2022**, 6(12): 1334–1338.

[29] Cavalleri, A., Ciani, G., Dolesi, R., Heptonstall, A., Hueller, M., Nicolodi, D., Rowan, S., Tombolato, D., Vitale, S., Wass, P. J., *et al.* A new torsion pendulum for testing the limits of free-fall for LISA test masses. *Classical and Quantum Gravity*, **2009**, 26(9): 094017.

[30] De Marchi, F., Pucacco, G., Bassan, M., De Rosa, R., Di Fiore, L., Garufi, F., Grado, A., Marconi, L., Stanga, R., Stolzi, F., *et al.* "Quasi-complete" mechanical model for a double torsion pendulum. *Physical Review D*, **2013**, 87(12): 122006.

[31] Bassan, M., Cavalleri, A., De Laurentis, M., De Marchi, F., De Rosa, R., Di Fiore, L., Dolesi, R., Finetti, N., Garufi, F., Grado, A., *et al.* A two-stage torsion pendulum for ground testing free fall conditions on two degrees of freedom. *Nuclear and Particle Physics Proceedings*, **2017**, 291: 134–139.

[32] Bassan, M., De Marchi, F., Marconi, L., Pucacco, G., Stanga, R., Visco, M. Torsion pendulum revisited. *Physics Letters A*, **2013**, 377(25–27): 1555–1562.

[33] Tu, Y. Precise measurement of period of torsion balance and the study of "abnormal mode" in the determining G. Master Thesis. Huazhong University of Science and Technology, **2004**. (in Chinese)

[34] Sun, J. G. On the perturbation of the eigenvalues of a normal matrix. *Mathematica Numerica Sinica*, **1984**, 6(3): 334–336. (in Chinese)

**Qifan Liu** is currently pursuing her Ph.D. degree at the National Key Laboratory of Aerospace Flight Dynamics (AFDL), School of Astronautics, Northwestern Polytechnical University. Her current research interests include dynamics analysis and guidance and control for spacecrafts.

**Xiaokui Yue** is a professor and doctoral supervisor at the School of Astronautics, Northwestern Polytechnical University. His main research areas include design of spacecraft, spacecraft flight dynamics and control theory, satellite navigation and integrated navigation technology, and space maneuvering and control.

**Zhaohui Dang** is an associate professor and doctoral supervisor at the School of Astronautics, Northwestern Polytechnical University. His main research areas include space orbital game technology, space artificial intelligence technology, and spacecraft formation flight technology.